Identification and quantification of caries from CBCT segmented images

Luiz G. K. Zanini[1], **Fátima L. S. Nunes** [1], **Izabel R. F. Rubira-Bullen** [1]

[1] Universidade de São Paulo (USP)

{luiz.kasputis, fatima.nunes, izabullen}@usp.br

Abstract. *Interproximal caries is a bacterial infection that occurs in the oral cavity, causing structural lesions between teeth. Diagnosis typically involves using radiographic techniques to capture images, but the use of Cone Beam Computed Tomography (CBCT) is still under-explored. This study explores CBCT, which acquires three-dimensional radiographic images, and employs two different image acquisition protocols to identify potential lesions. We developed a set of image processing techniques to segment three dental structures and accurately identify interproximal caries. Our results using classical metrics indicate an AUC of 0.928, a sensitivity of 87.33%, a precision of 88.50%, and a Jaccard Index of 0.7037. Our method effectively identifies lesions in dental structures, with the potential for practical assistance in diagnosing this disease.*

1. Introduction

Dental caries is a chronic infection that destroys dental tissues by fermentation of free sugars, resulting in a dynamic disease that causes demineralization and remineralization of dental hard tissues [Pitts et al. 2017]. Untreated dental caries can induce a risk of dental sepsis [Pine et al. 2006], which can cause intense pain and discomfort. Therefore, early diagnosis of this disease is essential to prevent tooth loss.

The cone beam computed tomography (CBCT) is a technique for capturing radiographic images in three dimensions (3D) [Gaalaas et al. 2016]. This imaging modality is used to diagnose and treat dental canals, demineralize teeth, low bone formation, and surgical treatment planning [Setzer et al. 2017]. Additionally, this technique can aid caries diagnosis when a radiologist identifies as an incidental finding [Felemban et al. 2020]. Therefore, incidental and suspicious caries lesions may be part of the final CBCT report issued by radiologists.

In the literature, the localization and classification of other diseases in computer tomography have been proposed in [Ezhov et al. 2021, Chen and Zhang 2017, Ahmed et al. 2017]. The authors of [Ezhov et al. 2021] proposed a method that used the individualization of teeth and segmentation. The caries were detected using U-Net [Ronneberger et al. 2015]; however, the method did not evaluate the segmentation results, but only the presence or absence of the disease. [Chen and Zhang 2017] proposed a segmentation process of dental disease employing image processing techniques. The method's final step used a threshold to identify the injured region. This work did not show metrics and focused only on the method. [Ahmed et al. 2017] combined unsupervised machine learning techniques using the mean threshold method and k-means to generate a segmentation. The study presented specific metrics to evaluate the results of segmentation; however, the work used computer tomography, unlike CBCT.

Although some approaches have been proposed in the literature for detecting and identifying caries, most studies do not have specific metrics for caries segmentation. Additionally, these articles do not thoroughly explore factors such as caries' severity. Therefore, our work aims to obtain specific segmentation metrics and present the results obtained at different levels of caries severity while also considering two CBCT imaging protocols.

This article aims to present a method based on image processing to segment dental structures and identify caries. In a previously published systematic review, [Schwendicke et al. 2019], it is possible to observe that most of the methods that processed CBCT images considered other objectives, such as the detection of periodontal diseases and tooth segmentation. However, these studies were not designed for caries segmentation. CBCT was mostly used as a complementary exam. Consequently, we proposed a new approach to aid the diagnosis of caries lesions, which can provide additional information from slices of CBCT, with the potential of expanding the diagnosis. Our method combines techniques to separate different portions of the tooth. With these portions separated, we used processing image techniques to identify evidence of caries.

2. Related work

Interproximal cavities develop in the areas of contact between teeth and their detection can be challenging, for accurate diagnosis the use of radiographic techniques is recommended [Braga et al. 2010]. Currently, image processing and deep learning have been used as the main methods for identifying interproximal caries.

The study conducted by [Naebi et al. 2016] employed image processing and particle swarm optimization methods to detect caries and dental restorations in 2D radiographic images. The [Bhan et al. 2016] research used pre-processing of bitewing images, including edge detection, thresholding and connected component labeling.

In caries detection using deep learning, the authors of [Srivastava et al. 2017] used a deep, fully convolutional neural network to identify the lesion in bitewing radiographic images. [Kumari et al. 2022] applied different techniques to enhance contrast and used Heuristically Modified Fusion-based Fuzzy C-Means for caries segmentation in dental x-ray images. The study of [Imak et al. 2022] used a multi-input deep convolutional neural network and reported an accuracy score of 99.13% for lesion detection on periapical radiography.

The authors of a systematic review [Mohammad-Rahimi et al. 2022] analyzed studies that aimed to detect caries using deep learning. The only paper that proposed the detection of caries using CBCT images was the study by [Ezhov et al. 2021]. The other works selected in that systematic review used different radiography modalities, such as panoramic radiography, bitewing radiography, and periapical radiography. These techniques offer a two-dimensional view, unlike CBCT images, which offer three-dimensional volumes.

As observed, several techniques have been proposed for caries segmentation using other radiographic modalities. However, CBCT images are not commonly used. With this gap in mind, we developed an image processing method to identify interproximal caries and achieve dental segmentation in this type of radiographic modality.

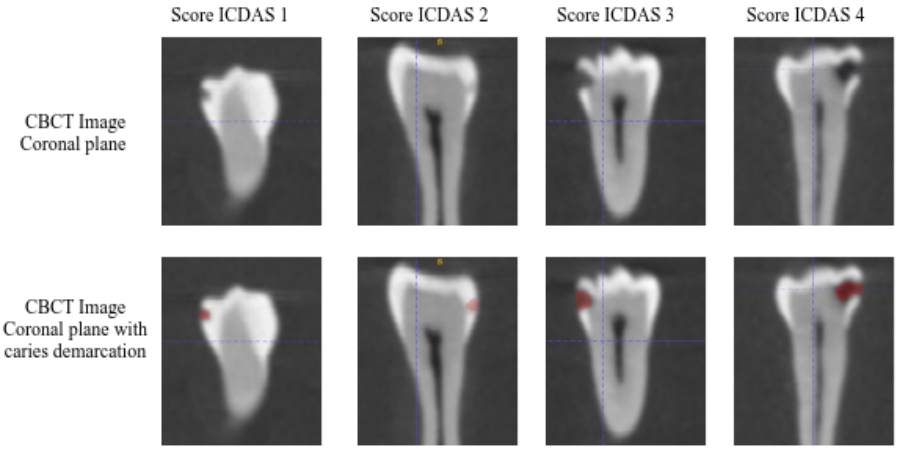

Figure 1. Examples of teeth with different scores based on the International Classification Caries Detection (ICDAS), figures with and without manual segmentation. The red region indicates the caries.

3. Material and Methods

We applied image processing techniques in our approach to segment CBCT images and identify caries in the image slices. In section 3.1, we explained our private dataset. We detailed our methodology for segmenting interproximal caries in sections 3.2, 3.3, 3.3, and 3.4. Finally, in section 3.5, we elucidated how we generated metrics from the segmented images.

3.1. Dataset

The data set contains 4008 images obtained from eight teeth with caries *ex-vivo*, and each tomography has 501 images (slices). Each tooth was classified according to the International Caries Detection and Assessment System (ICDAS). The CBCT was produced by using an Accuitomo 170 [Morita 2022] equipment, which offered two types of protocols: High Fidelity (HF), recommended for performing zoom reconstructions, and High Resolution (HR), recommended for delicate bone structures, such as the ossicular chain [Morita 2022].

Examples from images of the dataset are shown in Figure 1. The slices were manually segmented by an expert to generate a segmented ground-truth image set to evaluate the results of the techniques developed. The image base used in the experiments of this project was provided by the Faculty of Dentistry of Bauru (FOB) of the University of São Paulo.

3.2. Segmentation of tooth regions

A CBCT exam generates a 3D volume $I_{3D}(x, y, s)$, composed of two-dimensional (2D) images (slices) (Figure 2A), where (x, y, s) represents the intensity of the pixel in line x and column y, located in slice s.

The segmentation of structures aimed to develop a technique to verify the enamel discontinuity and the presence of concavities in the teeth. The distribution of pixels from CBCT changes according to the equipment. Considering this scenario, we applied a multimodal threshold [Tsai 1995] to all slices that compose I_{3D}.

The first step applied a Gaussian kernel G_σ convolution to I_{3D}. The acquisition of CBCT images captures ionizing radiation on the tissues, such that some noise can be also captured. Therefore, Gaussian Kernel was applied to $I_{3D}(x, y, s)$ to reduce the noise (Figure 2B). Besides, the application of the Gaussian kernel helps with the composition of the histogram [Tsai 1995] observed in Figure 3.

The next step was to segment each slice, considering three tooth structures. As the distribution of pixels is variable, we applied the multimodal thresholding technique. A histogram over the distribution of pixels from I_{3D} was calculated. We computed two locals minimums in this histogram corresponding to T_0 and T_1 (Figure 3). With these two local minimums, we applied a multimodal thresholding using T_0 and T_1, and segmented the resulting structures according to Equation 1.

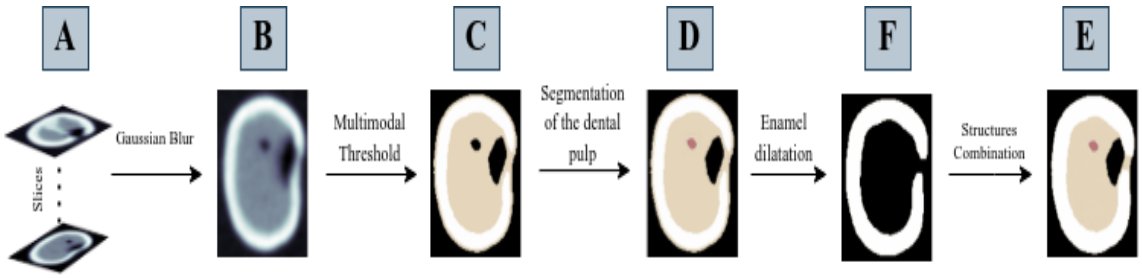

Figure 2. Segmentation of the dental structures. A) Representation of a CBCT exam. B) Application of the Gaussian filter. C) Initial separation of dental structures using multimodal thresholding. D) Application of growth region in the tooth pulp F) Application of morphological operation onto enamel. E) Final representation of the structure S_t.

Before applying Equation 1 to the $I_{3D}(x, y, s)$, we defined the element of the segmentation tooth. Where S_t is a 3D volume and represents the tooth segmentation. The values from S_t are respectively: 0.0 is the number that represents the background, 1.0 corresponds to the dentin material, 2.0 indicates the tooth enamel, and finally, value 3.0 denotes the pulp of the tooth.

$$S_t(x, y, s) = \begin{cases} 0.0 & \text{if } I_{3D}(x, y, s) < T_0 \\ 1.0 & \text{if } I_{3D}(x, y, s) >= T_0 \text{ and } I_{3D}(x, y, s) < T_1 \\ 2.0 & \text{if } I_{3D}(x, y, s) >= T_1 \end{cases} \quad (1)$$

After applying the multimodal thresholding (Figure 2C), we segmented the tooth pulp. This step is fundamental because the material has a low density and, consequently when we applied the algorithm for area delimitation (Section 3.3), this region could interfere. We first calculated the tooth center in each slice to determine the region where the root of the tooth is. For this, we calculated the image moment using the intensity of the pixels; it was determined $\overline{x}$ and $\overline{y}$ by Equation 2, where M_{ij} represents the moments from the x and y plane, and $x^i y^j$ is the influence of x or y in the computation of the moments.

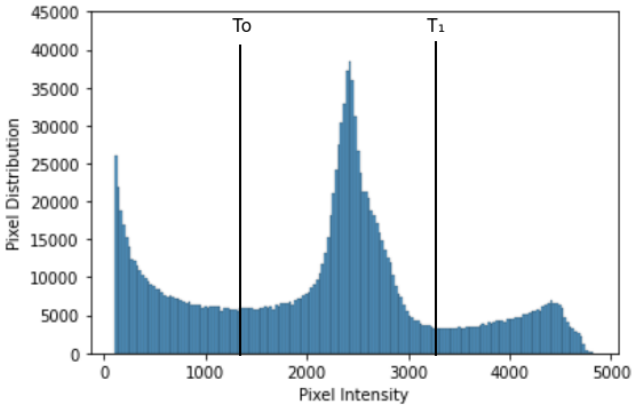

Figure 3. Distribution of pixels of a CBCT. We considered pixels larger than one hundred for visualization for this illustrative graphic since their representation would be impossible due to the unbalanced values.

$$
\begin{aligned}
M_{ij} &= \sum_{x}\sum_{y} x^i y^j I_{3D}(x,y) \\
\{\bar{x},\bar{y}\} &= \left\{\frac{M_{10}}{M_{00}}, \frac{M_{01}}{M_{00}}\right\}
\end{aligned}
\tag{2}
$$

We applied a region growing technique considering the center of the tooth as the initial seed, being delimited by the dentin material, as represented in Equation 3. The final process attributes value 3.0 to pixels related to the tooth pulp, resulting in the operation shown in Figure 2D.

$$
S_t(x,y,s) = \begin{cases} 3.0 & \text{if } S_t(x,y,s) \neq 1.0 \\ 1.0 & \text{else} \end{cases}
\tag{3}
$$

When multimodal thresholding is applied, the method can generate some segmentation failures, especially in the enamel region. Thus, in this scenario, we apply the morphological operation dilation in the regions whose pixels have values 2.0, according to Figure 2F. The next step is to join the dilated structure with S_t obtaining the result corresponding to Figure 2E.

In order to apply the techniques developed to extract caries considering concavities (Section 3.3) and discontinuity of dental enamel (Section 3.4), we created a region of interest (ROI). We computed the ROI in the slices in which tooth enamel is present. Thus, we went through slices from 0 to 501. We started searching for the first slice in which the enamel dental occurred (s_{min}) and the last slice in which tooth enamel appeared (s_{max}). Therefore, we had a range of slices s_{min} and s_{max}, to which the methods would be applied to extract regions of interproximal caries.

3.3. Caries extraction by concavities

The formation of caries causes the destruction of tooth enamel and of the structure of dentin. Our method searches for regions in which this material has been demineralized. We applied the techniques according to Figure 4 to identify evidence of caries.

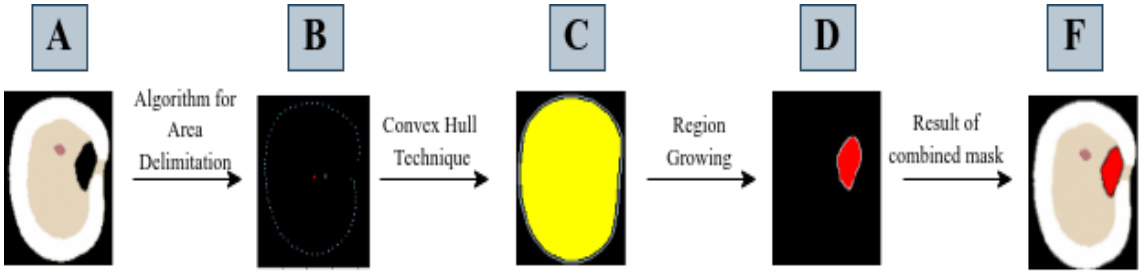

Figure 4. Caries extraction by concavities. A) Segmented Structures. B) Points generated by the region algorithm for area delimitation C) Region generated by the Hull convex method D) Application of growth region. F) Mask generation

We developed a method to get points that delimit the region in all slices from the CBCT images (Figure 4B). The Algorithm 1 shows the steps of our method, having as inputs S_t corresponding to the elements of the segmented structures and the center of the tooth ($\overline{x}$, $\overline{y}$). The algorithm starts searching at the midpoint ($\overline{x}$, $\overline{y}$), traversing a straight line with an angle that we change 0 to 360 degrees. This search occurs until it finds a value corresponding to $S_t = 0.0$, ending the search and storing the corresponding point as shown in Figure 4B. The method iterates over the ROI, returning the delimiter points (P_d) over all the slices in the ROI.

Algorithm 1 Algorithm for Area Delimitation

Input: $\overline{x}$, $\overline{y}$, S_t
Output: $delimitersPoints$
Initialization :
$delimitersPoints \leftarrow \{\}$
for $angle = 0$ to 360 **do**
  $x \leftarrow \overline{x}, y \leftarrow \overline{y}$
  $i \leftarrow 0$
  while $S_t(x, y) \neq 0.0$ **do**
    $x \leftarrow cos(angle) * i + \overline{x}$
    $y \leftarrow sin(angle) * i + \overline{y}$
    $i \leftarrow i + 1$
  end while
  $delimitersPoints.append(\{x, y\})$
end for
return $delimitersPoints$

The next step was to apply the convex hull [Sklansky 1982] method to P_d. The convex hull technique returns the intersection of all convex sets of P_d. The points not considered in P_d are stored as possible signs of caries (P_S). With points P_d we created a delimited area (D_A), which is the region corresponding to Figure 4C. Region D_A corresponds to the bounded area whereby the region growing technique can iterate. Therefore, we controlled how far the region could expand.

To generate the segmentation of caries, we applied the region growing method to P_S (Figure 4D), delimited by the region corresponding to D_A. In addition, we changed

the D_A $scale$ since the original area would cover all the points and regions that are not caries when we apply the region growing method. Parameter $scale$ is a value in the [0,1] interval, which allows increasing or decreasing the area considered for the region growing technique. Thus, when the $scale$ value is high, it can encompass regions that are not caries due to deformities or natural tooth wear. In turn, low values of $scale$ can restrict the region growing algorithm, which iterates over a smaller number of regions. Consequently, it is possible to reduce the value of false-positives, while increasing the value of false-negatives. Therefore, finding an ideal value of this parameter is necessary to obtain regions that correspond to caries. In section 3.5, we obtained a ROC curve and selected the best parameter for $scale$.

The area generated by the region growing method corresponds to the caries segmentation, as shown in Figure 4D. This area is added to the S_t structure (Figure 4F), thus generating the segmentation of this damaged region.

3.4. Caries extraction enamel by discontinuity

The method previously developed includes cases in which demineralization of dentin and enamel occurs. However, there are cases whereby the enamel material may not have been damaged enough to be very evident in CBCT images. Thus, in this phase, our method proposes identifying the regions where this dental enamel discontinuity occurred.

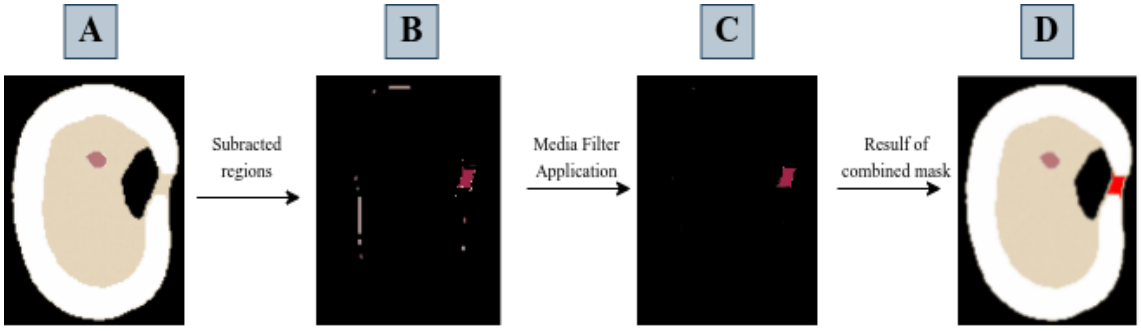

Figure 5. Segmentation of caries by enamel failure. A) Input S_t for the technique B) Subtraction of regions. C) Application of median filter D) Final result

The first step is based on iterating over ROI. In each iteration, the method seeks to verify if the dental enamel ring has already formed to identify signs of enamel discontinuity.

We used the depth-first search algorithm (DFS) to verify if the enamel ring formation occurred in a slice. We start the process by iterating over the ROI, starting the search at $\overline{x}$ and $\overline{y}$, which corresponds to the tooth center. The search algorithm moves to neighboring pixels; case $S(t)$ is different from 2.0, which corresponds to the enamel material. At the end of the search, it is possible to verify if the algorithm reached the edges of the image. If this condition is true, this slice has a discontinuity in the enamel and the slice is marked as s_{true}. Otherwise, the slice is marked as s_{false}.

We subtracted between the continuous and discontinuous regions to get the lesion region (Equation 4). Thus, in all the slices where this condition is true (s_{true}), we subtracted the last slice where the condition did not occur (s_{false}), returning the difference region (R_d) according to Equation 4.

$$R_d = S_e(s_{false}) - S_e(s_{true}) \tag{4}$$

The subtraction between the regions will be the area segmentation, providing the injured region. However, the subtraction of these regions can cause some noise, according to the result shown in Figure 5B.

The next step of the method consists in removing the noise caused by this subtraction. We used a median filter with a $5x5$ window applied to R_d (Figure 5C). The last step was to combine the segmentation generated from the previous technique with S_t, according to Figure 5D.

3.5. Experimental setup

The final segmentation is generated by combining the masks described in Sections 3.3 and 3.4. This combination produces a 3D segmentation that allows the evaluation of the severity of the lesion. We considered the segmentation generated for each slice to evaluate our method, comparing the results with the manual segmentation. In addition, we use CBCT exam with two types of protocols, HR and HF, to generate these images.

For each slice, we consider whether the caries segmentation corresponds to manual segmentation, generating for each tomography slice the values corresponding to a result of true-positive, false-positive, true-negative, and false-negative.

To evaluate the segmentation, we used the Jaccard index defined as Equation 5, where S corresponds to expert manual segmentation, and G corresponds to method segmentation. The Jaccard index has values between 0 and 1. If Jaccard = 1, this means that all pixels were correctly classified by the method developed.

$$J(S, G) = \frac{|S \cap G|}{|S| + |G| - |S \cap G|} \tag{5}$$

To generate the Receiver Operating Characteristics (ROC curve), we defined a parameter named $scale$ in the Section 3.3. In this scenario, we generated an area in which the Region Growing Method will iterate according to section 3.3. Therefore, we modified this area with the $scale$ parameter as follows from zero to one, with the step of 0.01.

4. Results and discussion

Figure 6 shows the ROC curve obtained from the variation provided by the $scale$ parameter. We sought to choose a value to reduce the false-positive rate and ensure a high true-positive rate. For this, we chose the value of $scale = 0.91$ for the HF protocol and $scale = 0.92$ for the HR protocol, which corresponds to an elbow in both ROC curves (indicated in the black rectangles in Figure 6).

In Tables 1 and 2, we present the results of the application of our method to eight decayed teeth with different International Caries Classification (ICDAS) and two protocols, HR and HF. The mean of all metrics was higher in the execution of the HR protocol, as can be seen in Table 1.

Only tooth 6 obtained better results in the HF protocol among all teeth. In general, the HR protocol provided a better structure for caries segmentation. The difference found

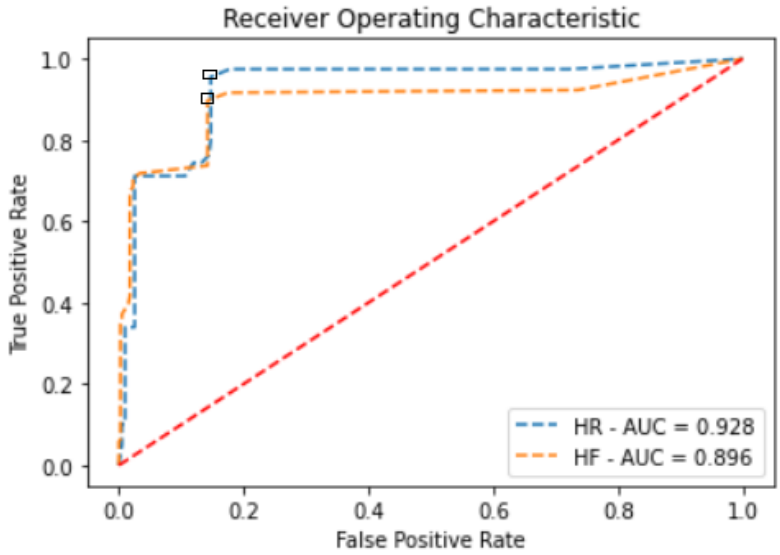

Figure 6. ROC curve generated from two protocols, High resolution (HR) and High Fidelity (HF). The black rectangle corresponding points with $scale = 0.91$ in HF and $scale = 0.92$ in HR.

in both protocols occurs in the separation of structures. Before we apply the multimodal thresholding, the pixel intensities have a difference; therefore, when we get two minimum locals in histograms, it directly affects the separation of structures and, consequently, the final segmentation of the method. Furthermore, the HR protocol had a better AUC value, as shown in Figure 6. The results are consistent with the manufacturer's specifications for providing images with delicate bone structures, which can be extended for caries identification.

None of the three studies that used 3D volumes differentiated carious lesions [Ezhov et al. 2021, Ahmed et al. 2017, Chen and Zhang 2017]. Additionally, these studies do not provide classic segmentation metrics that could allow a comparison. In our study, we present the differences between caries levels and highlight the difficulty of detecting caries in the initial stages, since they have a smaller injured region, as can be seen in Figure 1. The HR and HF protocols results show a lower sensitivity in ICDAS scores 1 and 2. In addition, the Jaccard index showed results higher in ICDAS scores 3 and 4. In [Ezhov et al. 2021], 4398 teeth were used to train a model with a context area. That model obtained sign caries with a sensitivity of 72.85% and specificity of 99.53%. Compared to [Ezhov et al. 2021], it is possible to observe that our study obtained similar specificity and sensitivity.

Deep learning has been proposed in works such as automatic caries detection [Srivastava et al. 2017, Kumari et al. 2022, Imak et al. 2022], but in other types of radiographic modalities (images 2D). The lack of data is one of the significant problems, since using deep learning approaches requires a dataset with a considerable quantity of samples. It is not possible to compare the results obtained in these approaches due to the difference between the 2D and 3D modalities

In this work, the use of image processing presented metrics such as AUC of 0.928, 88.50% of precision, and 99.58% of specificity, obtaining good results even with

Table 1. Table with results with $scale = 0.92$, using high resolution protocol. Highlights of the two best results.

Tooth	ICDAS	Accuracy	Sensitivity	Specificity	Precision	F1-Score	Jaccard index
1	1	99.6	77.78	**100.00**	**100.00**	87.50	58.01
2	1	99.0	93.55	99.36	90.62	92.06	71.23
3	2	98.6	75.00	98.99	54.55	63.16	50.67
4	2	99.4	80.00	99.80	88.89	84.21	50.71
5	3	**99.6**	90.00	**100.00**	**100.00**	**94.74**	78.47
6	3	99.2	**100.00**	99.17	84.00	91.30	**83.41**
7	4	**99.8**	**100.00**	99.79	96.67	**98.31**	**80.61**
8	4	98.4	82.35	99.57	93.33	87.50	69.91
Mean (sd)		99.20 ± 0.50	87.33 ± 9.91	99.58 ± 0.37	88.50 ± 14.79	87.34 ± 10.74	70.37 ± 15.59

a reduced number of samples. However, image processing involves some limitations, such as obtaining specific techniques for separating these structures and creating methods based on understanding the problem. Even if there are limitations, we show that a pipeline of image processing techniques can be enough to identify caries in CBCT images when the dataset contains few samples.

Table 2. Table with results with $scale = 0.91$, using high fidelity protocol. Highlights of the two or three best results

Tooth	ICDAS	Accuracy	Sensitivity	Specificity	Precision	F1-Score	Jaccard index
1	1	99.2	55.56	**100.00**	**100.00**	71.43	50.00
2	1	98.6	87.10	99.36	90.00	88.52	65.37
3	2	97.8	62.50	98.38	38.46	47.62	47.37
4	2	99.0	50.00	**100.00**	**100.00**	66.67	22.78
5	3	**99.6**	90.00	**100.00**	**100.00**	**94.74**	70.24
6	3	**99.4**	**100.00**	99.38	87.50	93.33	**92.43**
7	4	99.4	**96.55**	99.58	93.33	**94.92**	**79.13**
8	4	98.2	80.00	99.57	93.33	86.15	76.86
Mean (sd)		98.90 ± 0.64	77.71 ± 19.22	99.53 ± 0.53	87.82 ± 20.51	80.42 ± 17.01	65.52 ± 23.4

5. Conclusions

In this work we present a method based on the use of image processing techniques for caries segmentation. We obtained good results: 88.5% of precision 87.33% of sensitivity and 70.37 of Jaccard Index. It is possible to consider that the use of the method can be extended to other types of applications, such as the detection of other types of caries besides the interproximal and segmentation of the dental canal.

The results generated provide evidence that image processing techniques can segment and identify the injured region related to caries in CBCT images. The approach used was able to identify cases of interproximal caries. With the necessary adaptations, the project can provide the segmentation of each tooth.

The cited contributions can potentially achieve a technological impact since the system developed, after being validated, can be implemented in the clinical routine of dentists. Thus, the project results may also provide social and economic impact, as more accurate diagnoses may contribute to earlier interventions.

In future work we intend to use supervised learning to classify the slices involved in the segmentation process, providing a method capable of identifying and classifying the

lesion considering the ICDAS score. Providing accurate information about the severity of the lesion and determining whether immediate treatment or periodic monitoring is necessary is essential for ensuring the proper treatment of patients.

Acknowledgments

This work is supported in part by the Brazilian National Council for Scientific and Technological Development (CNPq grant number 307710/2022-0), the Coordination for the Improvement of Higher Education Personnel (CAPES Finance Code 001), Brazil, and Itaú Unibanco S.A. through the PBI program of the *Centro de Ciência de Dados* (C^2D) of Escola Politécnica at Universidade de São Paulo, and São Paulo Research Foundation (FAPESP) – National Institute of Science and Technology – Medicine Assisted by Scientific Computing (INCT-MACC) – grant 2014/50889-7.

References

Ahmed, S., Saifuddin, K. M., Ahmed, A. S., Aowlad Hossain, A., and Iqbal, M. T. (2017). Identification and volume estimation of dental caries using CT image. In 2017 IEEE International Conference on Telecommunications and Photonics (ICTP), pages 48–51.

Bhan, A., Goyal, A., Harsh, Chauhan, N., and Wang, C.-W. (2016). Feature line profile based automatic detection of dental caries in bitewing radiography. In 2016 International Conference on Micro-Electronics and Telecommunication Engineering (ICMETE), pages 635–640.

Braga, M. M., Mendes, F. M., and Ekstrand, K. R. (2010). Detection activity assessment and diagnosis of dental caries lesions. Dental Clinics of North America, 54(3):479–493.

Chen, R. and Zhang, H. (2017). Large-scale 3D Reconstruction with an R-based Analysis Workflow. In Proceedings of the Fourth IEEE/ACM International Conference on Big Data Computing, Applications and Technologies, BDCAT '17, pages 85–93, New York, NY, USA. Association for Computing Machinery.

Ezhov, M., Gusarev, M., Golitsyna, M., Yates, J. M., Kushnerev, E., Tamimi, D., Aksoy, S., Shumilov, E., Sanders, A., and Orhan, K. (2021). Clinically applicable artificial intelligence system for dental diagnosis with CBCT. Scientific Reports, 11(1):15006. Number: 1 Publisher: Nature Publishing Group.

Felemban, O. M., Loo, C. Y., and Ramesh, A. (2020). Accuracy of Cone-beam Computed Tomography and Extraoral Bitewings Compared to Intraoral Bitewings in Detection of Interproximal Caries. The Journal of Contemporary Dental Practice, 21(12):1361–1367.

Gaalaas, L., Tyndall, D., Mol, A., Everett, E. T., and Bangdiwala, A. (2016). Ex vivo evaluation of new 2D and 3D dental radiographic technology for detecting caries. Dento Maxillo Facial Radiology, 45(3):20150281.

Imak, A., Celebi, A., Siddique, K., Turkoglu, M., Sengur, A., and Salam, I. (2022). Dental Caries Detection Using Score-Based Multi-Input Deep Convolutional Neural Network. IEEE Access, 10:18320–18329. Conference Name: IEEE Access.

Kumari, A. R., Rao, S. N., and Reddy, P. R. (2022). Heuristically Modified Fusion-based Hybrid Algorithm for Enhanced Dental Caries Segmentation. In 2022 International Conference on Advances in Computing, Communication and Applied Informatics (ACCAI), pages 1–7.

Mohammad-Rahimi, H., Motamedian, S. R., Rohban, M. H., Krois, J., Uribe, S. E., Mahmoudinia, E., Rokhshad, R., Nadimi, M., and Schwendicke, F. (2022). Deep learning for caries detection: A systematic review. Journal of Dentistry, 122:104115.

Morita, J. c. (2022). 3D Accuitomo 170 | MORITA.

Naebi, M., Saberi, E., Fakour, S. R., Naebi, A., Tabatabaei, S. H., Moghadam, S. A., Bozorgmehr, E., Behnam, N. D., and Azimi, H. (2016). Detection of carious lesions and restorations using particle swarm optimization algorithm. International Journal of Dentistry, 2016:1–7.

Pine, C. M., Harris, R. V., Burnside, G., and Merrett, M. C. W. (2006). An investigation of the relationship between untreated decayed teeth and dental sepsis in 5-year-old children. British Dental Journal, 200(1):45–47. Number: 1 Publisher: Nature Publishing Group.

Pitts, N. B., Zero, D. T., Marsh, P. D., Ekstrand, K., Weintraub, J. A., Ramos-Gomez, F., Tagami, J., Twetman, S., Tsakos, G., and Ismail, A. (2017). Dental caries. Nature Reviews Disease Primers, 3(1):1–16. Number: 1 Publisher: Nature Publishing Group.

Ronneberger, O., Fischer, P., and Brox, T. (2015). U-Net: Convolutional Networks for Biomedical Image Segmentation. arXiv:1505.04597 [cs].

Schwendicke, F., Golla, T., Dreher, M., and Krois, J. (2019). Convolutional neural networks for dental image diagnostics: A scoping review. Journal of Dentistry, 91:103226.

Setzer, F. C., Hinckley, N., Kohli, M. R., and Karabucak, B. (2017). A Survey of Cone-beam Computed Tomographic Use among Endodontic Practitioners in the United States. Journal of Endodontics, 43(5):699–704.

Sklansky, J. (1982). Finding the convex hull of a simple polygon. Pattern Recogn. Lett., 1(2):79–83.

Srivastava, M. M., Kumar, P., Pradhan, L., and Varadarajan, S. (2017). Detection of Tooth caries in Bitewing Radiographs using Deep Learning. arXiv:1711.07312 [cs].

Tsai, D.-M. (1995). A fast thresholding selection procedure for multimodal and unimodal histograms. Pattern Recognition Letters, 16(6):653–666.